Title

Mechanisms of Cellular Proteostasis: Insights from Single-Molecule Approaches

Journal

Annual Review of Biophysics, 43(1)

ISSN

1936-122X

Authors

Bustamante, Carlos J
Kaiser, Christian M
Maillard, Rodrigo A
et al.

Publication Date

2014-05-06

DOI

10.1146/annurev-biophys-051013-022811

Peer reviewed

HHS Public Access

Author manuscript

Annu Rev Biophys. Author manuscript; available in PMC 2015 October 26.

Published in final edited form as:

Annu Rev Biophys. 2014 ; 43: 119–140. doi:10.1146/annurev-biophys-051013-022811.

Mechanisms of Cellular Proteostasis: Insights from Single-Molecule Approaches

Carlos J. Bustamante[1,2,3,4,5,6], **Christian M. Kaiser**[1,4,5], **Rodrigo A. Maillard**[1,5], **Daniel H. Goldman**[2,5], and **Christian A.M. Wilson**[1,5]

Carlos J. Bustamante: carlosjbustamante@gmail.com; Christian M. Kaiser: Kaiser@jhu.edu; Rodrigo A. Maillard: ram279@georgetown.edu; Daniel H. Goldman: dhgoldman@berkeley.edu; Christian A.M. Wilson: yitowilson@gmail.com

[1] QB3 California Institute for Quantitative Biosciences, University of California, Berkeley, California 94720-3220

[2] Department of Chemistry, University of California, Berkeley, California 94720-3220

[3] Department of Molecular and Cell Biology, University of California, Berkeley, California 94720-3220

[4] Department of Physics, University of California, Berkeley, California 94720-3220

[5] Jason L. Choy Laboratory of Single-Molecule Biophysics, University of California, Berkeley, California 94720-3220

[6] Howard Hughes Medical Institute, University of California, Berkeley, California 94720-3220

Abstract

Cells employ a variety of strategies to maintain proteome homeostasis. Beginning during protein biogenesis, the translation machinery and a number of molecular chaperones promote correct de novo folding of nascent proteins even before synthesis is complete. Another set of molecular chaperones helps to maintain proteins in their functional, native state. Polypeptides that are no longer needed or pose a threat to the cell, such as misfolded proteins and aggregates, are removed in an efficient and timely fashion by ATP-dependent proteases. In this review, we describe how applications of single-molecule manipulation methods, in particular optical tweezers, are shedding new light on the molecular mechanisms of quality control during the life cycles of proteins.

Keywords

force spectroscopy; worm-like chain; protein folding; chaperones; ribosome; proteases

INTRODUCTION

Cells employ a diverse set of strategies to maintain proteome homeostasis, or proteostasis: The cellular machinery for protein synthesis, including aminoacyl tRNA synthetases, translation factors, and the ribosome, cooperates to faithfully translate the genetic

DISCLOSURE STATEMENT

The authors are not aware of any affiliations, memberships, funding, or financial holdings that might be perceived as affecting the objectivity of this review.

information into functional polypeptides and tunes synthesis to meet demands and challenges. As soon as a nascent protein emerges from the ribosome, it begins to interact with molecular chaperones (37) and a variety of other factors (54) that contribute to proper folding, processing, and targeting. A subset of molecular chaperones protects the cell against the deleterious consequences of the unfolding and misfolding of proteins during their functional life. Once a protein is terminally inactivated, or no longer needed, specialized degradation machineries clear the cell of potentially toxic or undesired species (80). All these processes must be tuned and regulated to ensure cellular survival and fitness. Therefore, a mechanistic understanding of cellular proteostasis and its underlying dynamics is needed to understand how these processes are synchronized inside the cell.

Classical biochemical assays, or ensemble studies, have been conducted to study each of these processes. However, these methods often mask the heterogeneity inherent to populations of macromolecules, which are subject to random fluctuations when interacting with the thermal bath. Single-molecule (in singulo) studies (14) are a powerful approach to investigate the dynamic behavior and functional mechanisms of biological macromolecules. The information derived from single-molecule experiments provides direct insight into biological phenomena that cannot be obtained from ensemble measurements. Thus, single-molecule approaches have become invaluable tools complementary to more traditional approaches to study biological mechanisms.

Monitoring the behavior of individual molecules over time makes it possible to obtain not only the average behavior of the population but also to resolve rare events and detect the presence of short-lived states that are all but averaged out in ensemble measurements. The most widely employed single-molecule approaches are single-molecule fluorescence (56, 89) and single-molecule force spectroscopy (69). Through the latter it is possible to mechanically manipulate molecules in a highly specific manner. Single-molecule force spectroscopy studies using optical tweezers and their application to biological processes related to proteostasis are the focus of this review.

Atomic force microscopy (AFM), magnetic tweezers, and optical tweezers allow the direct application of mechanical forces on biological macromolecules. They also make it possible to measure these forces as well as those developed in the course of biological activity (for complete reviews about individual molecule manipulation techniques, see References 17 and 25). Together, these tools represent the most widely utilized techniques in single-molecule force spectroscopy. Other techniques, such as microneedle manipulation, biomembrane force probe, and flow-induced stretching, also allow measurement of forces at the single-molecule level, although their uses and versatility are significantly more restricted.

AFM has been widely used for studying protein folding at the single-molecule level (13, 31). Force is applied to a single molecule tethered between a surface and the tip of a cantilever by moving the surface using a piezoelectric stage. The deflection of a cantilever of a known spring constant serves as a readout of the force acting on the molecule. The advantages of AFM include a broad range of forces [10–10,000 piconewtons (pN)] and high spatial resolution (0.5–1 nm). In addition to its application for mechanical manipulations, AFM is also used to visualize biological molecules deposited on a surface. Impressively,

these two modi operandi can be combined in a single experiment (71). Recent advances in the time resolution that can be achieved in imaging mode have opened new avenues for applying AFM to study the dynamics of biological processes (52).

Magnetic tweezers are based on the interaction of a ferromagnetic object, typically a magnetic bead, with a magnetic field. The molecule of interest is immobilized between the magnetic bead and a surface. The force on the bead can be adjusted by varying the magnetic field, and the position of the bead is tracked by video microscopy. Of the three techniques mentioned above, magnetic tweezers have the lowest spatial resolution (5–10 nm); however, they allow access to the lowest force regime attainable with these methods (down to ~0.01 pN). Additionally, radiative heating of the sample and photodamage, which can present a concern in optical tweezers measurements, are absent in magnetic trapping. Because the ferrite cores in superparamagnetic beads often have irregular, nonspherical shapes, they often possess a small permanent dipole moment that can be used to apply torque through an external rotating magnetic field. Moreover, magnetic tweezers have the advantage of generating very stable force fields that can be applied simultaneously to many individual molecules in a single experiment.

Optical trapping allows one to apply force and manipulate individual molecules, as well as to measure the forces exerted during various biological processes. At Bell Laboratories, Arthur Ashkin discovered that microscopic particles can be stably trapped in a potential well formed by a focused laser beam (5, 6). By focusing such a laser beam through a microscope objective, a particle of high refractive index, such as glass or plastic, can be stably trapped by a light beam. The trapping mechanism results from the balance of two types of optical forces: scattering forces, which push the object in the direction of propagation of the light beam, and gradient forces, which attract the particle to the focal point in all three dimensions. When the gradient forces exceed the scattering forces, the particle is stably trapped. Generally, near-infrared lasers with wavelengths that are minimally absorbed by biological samples are used.

To create an optical trap, the laser beam is tightly focused by a high-numerical-aperture microscope objective lens. Such focusing creates the large spatial gradient in light intensity necessary to form a stable trap. To a first approximation, the trap behaves as a Hookean spring; a force acts on an object when it is displaced from the center of the trap, and this force can be calculated as the product of the spring constant of the trap, k, and the object displacement, Δx. This method has been replaced in some instruments by direct measurement of light momentum (85).

Mechanical forces are generated by a number of cellular processes, including DNA replication, transcription, translation, chromosomal segregation, protein folding and unfolding, translocation of proteins across membranes, cell locomotion, and protein degradation. Motor enzymes use the energy of ATP, GTP, or TTP binding or hydrolysis, or product release to generate mechanical work (2, 21). These motor enzymes, thus, couple a mechanical task—force or torque generation—to a thermodynamically favorable chemical reaction. The ability to apply external forces in a precisely defined manner provides a useful tool to study the mechanochemical transformations that accompany cellular processes and

obtain mechanistic insights about their operation. By monitoring the response of a molecule undergoing one of these processes to an applied force, it is possible to determine the thermodynamic and kinetic parameters of the reaction. In particular, by systematically varying the force, the ATP concentration, or its hydrolysis products (ADP and phosphate), it is possible to determine the location of the force-generating step in the reaction pathway (15) and ultimately formulate a comprehensive understanding of the mechanisms of their mechanochemical operations.

Any process that comprises a change in molecular extension can in principle be monitored and altered with optical tweezers. For example, the end-to-end length of a compactly folded biopolymer is much shorter than that of the unfolded polymer under tension. This enables direct observation of transitions between conformational states of proteins and ribonucleic acids(RNAs). Moreover, because the application of force tilts the potential energy surface associated with the folded and unfolded states (15), its effect is to perturb the equilibrium between those states and drive transitions between them. The folding and unfoldingof small globular proteins is an example of a two-state process because proteins typically fold and unfold cooperatively. The equilibrium constant, K_{eq}, governing the distribution of the folded and unfolded states depends exponentially on the force applied to the ends of the polypeptide according to

$$ln \quad K_{eq}(F) = -\frac{\Delta G^0 - F\Delta x}{k_B T}, \quad 1$$

where ΔG^0 represents the standard free energy of folding, Δx is the change in molecular extension in the unfolding process, *kg* is the Boltzmann constant, and *T* represents the temperature. The application of force not only affects the heights and positions of the folded and unfolded states along the reaction coordinate but also the relative height of the barrier separating them [see the sidebar titled Dependence of the Rate Constant on Force (Bell Equation)]. Thus, a continuously increasing force acting on a folded protein eventually leads to the unfolding of the molecule-and a corresponding increase in the extension of the molecule-when the system crosses the energy barrier (see **Figure 1*a***).

The most likely unfolding force, $\overline{F_U}$, is dictated by the structure of the protein and the axis along which force is applied. In this nonequilibrium experiment, $\overline{F_U}$ also depends on the loading rater (with $r \equiv dF/dt$), i.e., the rate at which the force is applied:

$$\overline{F_U} = \frac{k_B T}{\Delta x^{\ddagger}} \quad ln \quad \frac{\Delta x^{\ddagger} \cdot r}{k_0 \cdot k_B T}, \quad 2$$

DEPENDENCE OF THE RATE CONSTANT ON FORCE (BELL EQUATION)

Bell (3) was the first to phenomenologically describe the dependence of reaction kinetics on force. For the analysis of kinetic data, Bell's model (3) predicts an experimental dependence of the rate constant on the external force:

$$k = k_m k_0 e \left(\frac{\Delta x^{\ddagger} F - \frac{1}{2} K \left(\Delta x^{\ddagger} \right)^2}{k_B T} \right),$$

where k_m represents the contribution of experimental parameters, such as the bead size, trap stiffness, and handle length, to the observed rate; *ko* is the intrinsic rate constant of the molecule in the absence of force; F is the force; $\Delta x^{\ddagger}$ is the distance to the transition state; K is the effective spring constant of the system; k_B is the Boltzmann constant; and T is the absolute temperature. In this notation, the applied force and effective spring constant of the system are positive, and the distance to the transition state is positive from the folded state to the unfolded state but negative from the unfolded state to the folded state. Bell's model emphasizes that the parameters k_0, k_m and K determine the absolute rate constants but are not easily deconvoluted, making any interpretation of the absolute rate constants difficult (**Figure 2**) (30).

where $\Delta x^{\ddagger}$ is the distance to the transition state for the unfolding reaction, and k_0 is the unfolding rate at zero force. High loading rates drive the system further from equilibrium than low loading rates, resulting in higher unfolding forces. Thus, many features of the energy landscape that describe the folding of a protein can be directly determined from force spectroscopy measurements.

FORCE DEPENDENCE OF FOLDING AND UNFOLDING RATES

Based on Kramers's theory (55), a method has been derived to extract force-dependent lifetimes from unfolding force distributions (27):

$$\tau(F) = \tau_0 \left(1 - \frac{v F x^{\ddagger}}{\Delta G^{\ddagger}} \right)^{1 - \frac{1}{v}} e^{-\beta \Delta G^{\ddagger}} \left[1 - \left(1 - \frac{v F x^{\ddagger}}{\Delta G^{\ddagger}} \right) \right]^{\frac{1}{v}}.$$

In this expression, F is force, $x^{\ddagger}$ is the distance to the transition state, τ_0 is the lifetime, and $\Delta G^{\ddagger}$ is the apparent free energy of activation in the absence of an external force. The scaling factor v specifies the nature of the underlying free-energy profile: $v = 1/2$ corresponds to a harmonic well with a cusp-like barrier, or equivalently a harmonic barrier with a cusp-like well; $v = 2/3$ corresponds to a potential that contains linear and cubic terms; and for $v = 1$, Bell's formula [see the sidebar titled Dependence of the Rate Constant on Force (Bell Equation)] is recovered. Using this theory, one can extract the height of the free-energy barrier, the distance to the transition state, and the rate constant at zero force. These kinetic parameters have proven useful in describing the intrinsic properties of a number of proteins (47, 96).

Recent advances in theoretical biophysics have introduced powerful tools for the interpretation of data from single-molecule force spectroscopy experiments. This is illustrated by the development of an approach to analyze force-induced macromolecular

unfolding experiments (27) on the basis of Kramers's theory of diffusion over a barrier (see the sidebar titled Force Dependence of Folding and Unfolding Rates) (55). Using this theory, it is possible to extract the height of the free-energy barrier for folding and unfolding transitions, the distance to the transition state, and the unfolding rate constant at zero force. These kinetic parameters have proven useful in describing the folding/unfolding transitions of a number of proteins (47, 96). The expanding arsenal of analytical tools now also includes methodologies for extracting equilibrium thermodynamic parameters from nonequilibrium measurements (24, 44) and a comprehensive framework for extracting information about folding energy landscapes from pulling experiments (38). The concomitant development of experimental and analytical tools has provided an added impulse to the single-molecule field.

PROTEIN SYNTHESIS

The ribosome is a highly complex molecular machine that synthesizes proteins following the information contained in messenger RNA (mRNA) templates. It liaises with a number of other components to faithfully translate the genetic code into polypeptides and to safeguard accurate protein synthesis, folding, and maturation (72, 79, 97). The process of translation can be broadly divided into the three stages of initiation, elongation, and termination. Each of these stages comprises a number of distinct steps (or a series of repetitive steps in the case of elongation). Individual elongation steps involve a number of events, such as conformational transitions or binding and unbinding of elongation factors that are governed by specific rate constants. Therefore, even if two or more ribosomes are synchronized at the beginning of protein synthesis, they will rapidly lose synchrony as they proceed along the reaction path of translation. The power of single-molecule approaches lies in overcoming the ensemble averaging that necessarily results when observing nonsynchronized molecular populations. Hence, mechanistic aspects of ribosome function have been the subject of many informative single-molecule studies.

Optical tweezers have been utilized to follow the movement of single ribosomes along mRNA templates (93). This approach revealed how the ribosome employs two different mechanisms to interact with mRNA secondary structures (76), which often function as regulatory elements that modulate protein translation. Although the number of optical tweezers studies of translation remains limited to date, other single-molecule techniques have also yielded valuable insights about the mechanisms underlying translation elongation. In particular, fluorescence-based single-molecule approaches (in conjunction with the groundbreaking progress in high-resolution structural elucidations) have greatly contributed to a mechanistic understanding of the dynamics during translation. A number of excellent review articles summarize the striking progress in this field and illuminate it from different angles (4, 12, 32, 75, 89).

DE NOVO PROTEIN FOLDING

Single-molecule experiments offer a number of advantages that make them ideally suited to complement ensemble measurements for studying protein folding and unfolding. By applying force along a well-defined axis, folding and unfolding transitions in a single

protein molecule can be studied in a time-resolved manner, yielding kinetic information. In addition, it is possible to obtain equilibrium information from single-molecule experiments performed under nonequilibrium conditions using recently derived fluctuation theorems (24, 44). These theoretical advances have been applied to the analysis of single-molecule experiments involving the unfolding of protein and RNA molecules (**Figure 1**) (22, 57, 83).

The direct observation of structural transitions associated with protein folding also makes it possible to unambiguously distinguish on-pathway from off-pathway intermediates (19, 86). Folding intermediates are identified and distinguished not only by their molecular extension but also by their kinetic properties. The latter property has become increasingly useful with the recent development of analytical tools based on hidden Markov model analysis (30, 47, 86). Because force acts locally as a denaturant, it can be applied to a specific region of a protein or macromolecular complex while not affecting the global stability of the complex (47, 83). Furthermore, the reaction coordinate for unfolding can be altered by changing the pulling axis. In a recent example, this locality and directional flexibility have been exploited to probe the energetic coupling between subdomains in the T4 lysozyme (**Figure 1**) (83). Optical tweezers have also been used to probe the mechanical properties of amyloid fibrils, yielding insights into the molecular interactions underlying disease states (26). Optical tweezers provide a powerful tool to study protein folding, particularly in combination with recently developed analytical tools.

Despite great progress toward a better understanding of protein folding, relatively little is known about how proteins fold in the context of their synthesis by the ribosome. The vectorial nature of protein synthesis and the environment of the ribosome likely influence this process of de novo folding. Mechanistic studies of de novo folding have been mainly limited to theoretical approaches and computational methods owing to the technical challenges of such experiments both in bulk and at the single-molecule level. Statistical mechanics considerations have predicted that conformational confinement both stabilizes the native state and accelerates folding rates (99). By contrast, molecular dynamics simulations have shown that confinement in the context of the ribosome does not lead to increased folding rates (28). In fact, computational work suggests that close proximity to the ribosome may increase the free-energy barrier of folding in some proteins, effectively resulting in decreased folding rates (70).

A number of experimental studies have investigated the stability and the dynamics of nascent polypeptides. Some limited folding can begin even before the nascent protein emerges from the tunnel exit: Mass-tagging studies utilizing a transmembrane segment of a human voltage-gated potassium channel, Kv1.3, revealed that distinct regions within the ribosomal exit tunnel promote a compaction of the nascent chain (58) and can permit limited tertiary structure formation (53). Even though it is not clear to what degree these structures generally persist outside the specific environment of the ribosome exit tunnel, they highlight the importance of interactions between accessible ribosomal surfaces and nascent polypeptide residues. Elegant fluorescence resonance energy transfer (FRET) studies have revealed that the nascent polypeptide can acquire structure deep inside the exit tunnel, which results in regulation of translational elongation (95). Recent cryoelectron microscopy studies

(9–11) are beginning to shed light onto the molecular interactions that mediate cross talk between the ribosome and the translation product.

Upon leaving the narrow ribosome exit tunnel, the nascent protein becomes structurally more dynamic (29) and can undergo tertiary structure formation. Once a foldable unit has emerged, it can acquire its native structure before the nascent polypeptide is released from the ribosome. This process has been demonstrated most impressively by an approach using nuclear magnetic resonance spectroscopy to probe the structure of isotopically labeled nascent polypeptides (42, 43). These experiments also suggested that the ribosomal environment affects the stability of the folded protein. In addition to effects that are directly related to the ribosomal environment, interactions of the nascent chain with other cellular macromolecules (72) and ligands (50) determine how the proteins proceed toward their native state in the cell.

Elongation rates along the mRNA vary but do not exceed 20 amino acids per second (aa/s) (73). The synthesis of even small proteins or individual protein domains requires several seconds. Small proteins typically fold within milliseconds to seconds in vitro. Thus, folding begins cotranslationally, but the nascent polypeptide cannot acquire its stable native structure because not all of the sequence is available for folding yet. How do nascent proteins then avoid becoming trapped in nonnative structures when they can begin to fold before the information specifying the stable native structure is available? There is ample evidence that cotranslational structure formation occurs in nascent polypeptides and that the particular environment of the ribosome–both inside (94) and outside (98) the exit tunnel—affects the stability of folded structures. It is less clear, however, how these changes affect the actual folding transitions. It has not been possible to apply the suite of biophysical techniques utilized in protein folding studies to ribosome-bound nascent chains. For instance, spectroscopic techniques such as tryptophan fluorescence, circular dichroism, or hydrogen exchange spectroscopy cannot resolve the signal of the nascent polypeptide against the large background contributed by the ribosome, which itself comprises more than 50 proteins. Similarly, denaturing conditions typically used to perturb the stability of the native state for in vitro refolding studies, including elevated temperatures and high concentrations of chaotropes, cannot be selectively applied to avoid disrupting the integrity of the ribosome. Thus, novel experimental approaches are required to resolve the folding dynamics of nascent polypeptides in the native environment of the ribosome.

Mechanical force acts as a local denaturant and when applied across specific residues within a protein sequence permits the unfolding of defined regions within a folded structure (83). Therefore, single-molecule force spectroscopy offers a unique approach to study nascent chain folding by allowing selective denaturation of the nascent protein while keeping the ribosome intact. The suitability of this approach was demonstrated in a recent study using optical tweezers (47). To implement the experimental setup, stalled ribosome–nascent chain complexes were immobilized between polystyrene beads (**Figure 3**), and tension was applied to individual T4 lysozyme nascent chains. When the entire sequence of the T4 lysozyme is present outside the ribosomal exit tunnel, the protein is capable of adopting its native structure. Interestingly, the ribosome does not appear to alter the unfolding pathway induced by the application of an external force; a recently developed approach to analyze

force spectroscopy data based on Kramers's theory (see the sidebar titled Force Dependence of Folding and Unfolding Rates) (27) revealed that the mechanical unfolding energy landscapes for the ribosome-bound and the free protein are very similar. Thus, the ribosome does not affect the rate of native state unfolding in these experiments.

In contrast, the ribosome has a pronounced effect on nascent chain folding. In close proximity to the ribosomal surface, T4 lysozyme folding is decelerated by more than two orders of magnitude relative to the free protein. The folding rates increase with increasing separation between the nascent protein and the ribosome, suggesting that this modulation of folding by the ribosome is restricted to newly synthesized proteins in the proximity of the ribosome surface. Increasing the ionic strength of the buffer solution accelerated folding rates of the ribosome-bound protein but did not affect those of the free protein. This result indicates the importance of electrostatic interactions between the negatively charged surface of the ribosome and charged residues in the nascent polypeptide. Because virtually all proteins contain charged residues, these electrostatic interactions provide a general mechanism for modulating folding by biasing the conformational ensemble of the nascent polypeptide (92).

Although the ribosome modulates the folding kinetics of the T4 lysozyme, it does not change its folding pathway; the protein folds through an on-pathway intermediate both on and off the ribosome. In combination with a Bayesian hidden Markov model approach for data analysis, the single-molecule experiments revealed that the ribosome selectively decelerates a specific step during folding, namely the final transition from the intermediate to the native state. What advantage for de novo protein folding is conferred by a deceleration of folding rates? T4 lysozyme fragments were created that mimicked transiently occurring species before synthesis was completed. These fragments aggregate in vitro and were observed to misfold in single-molecule experiments. Strikingly, this is not observed in ribosome-bound nascent polypeptides. Thus, the ribosome prevents the formation of misfolded states in incompletely synthesized polypeptides, presumably through the kinetic mechanism discussed above. It is interesting to speculate that this process may provide sufficient time for the synthesis of a complete domain (or foldable unit) so that folding is attempted only once all the necessary information is available.

MOLECULAR CHAPERONES

In the cell, molecular chaperones work in concert with the ribosome to guide newly synthesized proteins to their native states (37). In fact, the ribosome appears to orchestrate how an ensemble of folding and targeting factors interacts with the nascent translation product in a productive fashion (72). Structural and biochemical studies have elucidated many critical aspects of chaperone function and regulation. Many chaperones, such as Hsp90 and the cylindrical chaperonins, are structurally and conformationally complex, making mechanistic studies challenging. Electrokinetic trapping (45) and single-molecule fluorescence approaches (67, 77, 78) have proven particularly useful in understanding the rich dynamic behavior of some molecular chaperones.

Single-molecule experiments using both fluorescence (20, 39, 51, 88) and force spectroscopy approaches (8, 64) are beginning to provide a mechanistic understanding of how client protein folding is modulated by chaperones. A number of chaperones act cotranslationally. The uniquely bacterial protein Trigger factor is activated by binding to the ribosome and is the first chaperone to contact the nascent polypeptide during translation. Trigger factor engages with nascent proteins preferentially through hydrophobic motifs (46). The methodological advances described above now enable experiments that probe the changes in the folding energy landscape of nascent proteins by Trigger factor (64). It will be exciting to see how chaperone activity for nascent polypeptides is organized and regulated by the ribosome. Recent advances in instrumentation have achieved the combination of ultrahigh-resolution optical trapping with single fluorophore detection capabilities (23), which will make understanding the complex interplay among the ribosome, the molecular chaperones, and the elongating nascent protein possible.

PROTEIN QUALITY CONTROL BY ATP-DEPENDENT PROTEASES

The process of controlled protein degradation is critical for the maintenance of cellular homeostasis in all organisms. Nonfunctional and potentially cytotoxic protein fragments are generated when ribosomes stall during translation before reaching a stop codon on the mRNA. If synthesis and folding are completed successfully, proteins need to be removed when they either misfold and aggregate (40) or when they are no longer needed, as in the case of regulatory proteins involved in cell division, chromosome replication, and transcription (1, 18, 35, 84). The protein degradation task is strictly regulated and mainly performed by ATP-dependent proteases. These ubiquitous, energy-dependent enzymes recognize protein substrates and degrade them in a timely and efficient fashion.

All ATP-dependent proteases share a common structural design (80) made up of two major components: a barrel-shaped peptidase with active sites sequestered deep inside its cavity (87) and a hexameric, ring-shaped ATPase of the AAA+ superfamily that uses the energy of ATP binding and hydrolysis to recognize and deliver the protein substrate into the associated peptidase (**Figure 4*a***) (33). The ATP-dependent protease ClpXP from *Escherichia coli* has served as a model system and has yielded many important operating principles of this family of proteins (60–63). Short peptide sequences, such as the ssrA tag, mediate the initial binding of protein substrates to loops within the axial pore of the ClpX ring (36, 61–63, 82). The ssrA tag is encoded by a special type of RNA named small stable RNA A, which rescues the ribosome during translation by adding an 11-codon degradation tag followed by a stop codon (91). After recognizing its protein substrate, ClpX translocates the protein through its central processing pore into ClpP. Because the diameter of the ClpX pore is very narrow (~10–15 Å), it was proposed that ClpX uses the energy of ATP to mechanically unfold the protein substrate before translocating it into ClpP. In fact, for mechanically stable substrates, ClpXP consumes hundreds of ATP molecules before successfully unfolding, translocating, and degrading the protein substrate (48). ClpXP is able to temporarily disengage and reengage hard-to-unfold protein substrates, which manifest as the enzyme temporarily slipping on the polypeptide track (48, 49). The ability to slip is a critical property of this group of enzymes because it allows them to reengage mechanically stable substrates multiple times until an unfolding attempt is successful (49, 65).

The direct observation of mechanical force generation by an ATP-dependent protease during substrate unfolding and translocation has been only recently achieved. By using a dual-trap optical tweezers instrument (68), two groups independently developed single-molecule assays to monitor—in real time—the unfolding and translocation of polypeptide substrates by individual ClpXP molecules (7, 59). In this experimental geometry, protein unfolding and translocation by ClpXP proceeded in the C- to N-terminal direction. Aubin-Tam et al. (7) used filamin A domains 1–8, whereas Maillard et al. (59) used substrates based on fusions of green fluorescent protein (GFP) and permanently unfolded I27 titin domains (**Figure 4*b***).

After successful substrate engagement, the molecular trajectories of ClpXP activity displayed sudden extension gains, or rips, followed by slower decreases in extension. Rips correspond either to the cooperative unfolding of an individual protein substrate or to the temporal disengagement of the substrate (i.e., a motor slip on a partially translocated polypeptide). The decrease in extension reflects the translocation of the unfolded protein substrate through the narrow processing pore of ClpXP. **Figure 4*c*** shows molecular trajectories wherein ClpXP unfolded and translocated a substrate consisting of two tandem GFP molecules separated by two permanently unfolded I27 titin domains (59).

ATP-dependent proteases must cope with a diverse set of protein substrates with variable mechanical stabilities and topologies (81). For instance, ClpXP unfolded in a single rip a small protein substrate consisting of a single domain (filamin A), which occasionally displayed a short-lived intermediate with a lifetime of less than 5 ms (**Figure 5*a***) (7). The force-induced mechanical unfolding by ClpXP of GFP, a protein with a complex topology, reproducibly displayed a well-defined intermediate state (59) with a lifetime of ~180 ms (**Figure 5*b***). Using the worm-like chain expression for the extension of a polymer molecule subjected to an externally applied force (see the sidebar titled Worm-Like Chain Behavior of a Protein) (16), it was possible to estimate the number of amino acids involved in the first unfolding event. These amino acids were mapped onto the structure of GFP to determine that β-strands 11 → 7 were extracted from GFP under the action of ClpXP. The remaining, short-lived intermediate most likely unfolds spontaneously because it is located far from ClpXP (**Figure 5*c***). However, it was observed that ClpXP is able to translocate before the unfolding intermediate is fully unraveled (**Figure 5*b***), indicating that the mechanical pulling generated by ClpXP as it translocates the unfolded chain may contribute to the further destabilization of the GFP intermediate.

WORM-LIKE CHAIN BEHAVIOR OF A PROTEIN

The worm-like chain equation describes the dependence of force on the molecular extension of a flexible polymer in a thermal bath. A long polymer tends to contract to maximize conformational entropy. The resulting force is given by (16)

$$F = \frac{k_B T}{p}\left[\frac{1}{4}\left(1 - \frac{x}{L_C}\right)^{-2} - \frac{1}{4} + \frac{x}{L_C}\right],$$

where p is the persistence length of the chain (p = 0.65 nm is used for proteins) (19), x is the end-to-end extension, and L_C is the contour length [calculated by multiplying the number of amino acids (aa) by 0.36 nm/aa]. Incalculating changes in contour length during folding or unfolding reactions, the end-to-end length between the attachment points in the folded protein (obtained from a high-re90lution structure) must be subtracted from the unfolded contour length.

Additional insight into the mechanism of protein unfolding by ClpXP was obtained by analyzing the unfolding rate of the substrate. Aubin-Tam et al. (7)observed that the distribution of unfolding times differs significantly between filamin A domains, even though they are structurally very similar. The unfolding times of natively folded GFP by ClpXP varied from 1 s to 60 s, following a single exponential distribution with a time constant of ~9 s (**Figure *5c***) (59). The unfolding rate of protein substrates likely depends on several factors, including the mechanical stability of the substrate's local structures encountered by ClpXP (48, 65) and the type of polypeptide sequence preceding the folded protein. It is possible that a particular amino acid type favors a stronger interaction with ClpXP and therefore allows a better grip on the polypeptide chain during the substrate unfolding process (41, 90).

After unfolding its protein substrate, ClpXP translocates the polypeptide through its central processing pore into ClpP. In single-molecule trajectories, the decrease in extension over time (slope) represents the velocity of an individual ClpXP molecule over the unfolded polypeptide (**Figure 4*c***). In most trajectories, continuous translocation is observed, suggesting a motor of high processivity. However, in some trajectories, the translocation of the motor over the polypeptide was seen to halt temporarily. These regions of the trajectory of near-zero velocity were identified as "pauses" (**Figure 4*c***). Aubin-Tam et al. (7) and Maillard et al. (59) obtained a pause-free translocation velocity of ClpXP by removing the pauses during data analysis. By subjecting the motor to different degrees of opposing load, it is possible to probe the response of the motor's pause-free velocity to force. ClpXP translocates polypeptides at a nearly constant pause-free velocity of 6 nm/s up to forces near 13 pN (**Figure *6a***). Above 13 pN, the pause-free translocation velocity begins to decrease, enabling the estimation of a stall force of ~20 pN for ClpXP (7, 59). The 20-pN stall force probably represents a lower bound of the maximum amount of mechanical force that ClpXP can generate to unfold its protein substrates.

One unique aspect of ATP-dependent proteases is that, unlike polymerases and cytoskeletal motors, they move along a highly flexible and extensible track. For instance, a track made of unfolded polypeptide doubles its end-to-end length (extension) when stretched from ~4 pN to ~12 pN. Thus, ClpXP maintains a constant pause-free translocation velocity of 6 nm/s throughout the force range of 4 to 12 pN, whereas its velocity in amino acids per second decreases monotonically from ~60 aa/s at 4 pN to 30 aa/s or less at forces above 12 pN (**Figure *6b***). This notion is consistent with a model in which ClpXP maintains a fixed translocation step that translates into a smaller number of amino acids per step as the opposing force increases. In fact, ClpXP has been observed to take steps of 1 nm, although 2 and 3 nm are the most frequently detected (59). This constant stepping in nanometers is

probably determined by the geometry of the motor and may reflect the amplitude of the power stroke of a single subunit (1-nm step) or multiple subunits (2- and 3-nm steps) during polypeptide translocation (**Figure 6*c***). The observation of 2- and 3-nm steps suggests a coordinated, near-simultaneous stepping of two or three motor subunits (59), whereas the 1-nm step may correspond to the fundamental step size of a single ClpX subunit (7, 59).

Previous reports have shown that ClpXP and other ATP-dependent proteases process a large number of client proteins (81), indicating that these degradation machines must cope with structurally and functionally diverse protein substrates that are not only in a soluble conformation but also in hyperstable states as in the case of protein aggregates. Is the stall force of ~20 pN, determined for ClpXP, large enough for the enzyme to unfold all its substrates? This question can be answered by analyzing the loading rate at which the force is applied by the motor (Equation 2 in the Introduction). The most likely force at which a protein unfolds scales as the log of the loading rate (15). In the case of ClpXP, the loading rate was estimated to be ~0.15 pN/s, which is five orders of magnitude smaller than the loading rate used in AFM unfolding experiments (66, 74). This large difference in loading rates implies that proteins that display high mechanical stability in AFM pulling experiments (such as GFP) will unfold at forces at least five times smaller under the action of ClpXP (see Equation 2). Future experiments of the type described here should establish if the close proximity of ClpXP with its target also contributes to destabilizing the protein substrate for efficient unfolding.

Most biophysical and biochemical studies on ATP-dependent proteases have been done with the AAA+ ATPase in complex with the peptidase chamber (for a review see 80). This is the case for ClpXP, even though it is well established that, inside the cell, ClpX also functions alone as an unfoldase. For example, ClpX drives protein-remodeling reactions that allow the dissociation and release of the MuA transposase from the DNA after recombination (1). It was also possible to characterize the motor properties of ClpX in the absence of ClpP by single-molecule methods (59). The pause-free translocation velocity curve for ClpX displayed the same force dependence observed for ClpXP, with a similar stall force of ~20 pN. However, the mean translocation velocity for ClpX was ~25% higher than that of ClpXP (**Figure 6*a***). This increase in velocity probably reflects the ~30% higher ATPase rate observed for ClpX when the motor is not bound to the peptidase ClpP (60).

Maillard et al. (59) found a nonlinear relationship between the ATPase rate and the mean GFP unfolding time when the investigators compared single-molecule data from ClpX and ClpXP. Although ClpX had about a 30% increase of ATPase rate relative to ClpXP, the motor alone unfolded GFP five times faster than when it was bound to the peptidase ClpP, with an unfolding time constant of 1.7 s (59). Previous bulk biochemical studies proposed that degradation of GFP by ClpXP requires four or more consecutive ATP-binding and hydrolysis events. This requirement of multiple ATP-binding and hydrolysis events results in the nonlinear relationship between the ATPase rate and GFP unfolding and degradation (63). In optical tweezers translocation experiments, the ATPase rate of the motor can be related to its pause-free translocation velocity “v” using the following equation: $v = d \cdot k_{cat} \cdot \varepsilon$, where d is the motor step size, k_{cat} is the motor turnover rate, and ε is the coupling coefficient, i.e., the probability that the motor steps in a given hydrolysis cycle (21). Thus,

the consecutive ATP-binding and hydrolysis events required to successfully unfold and degrade GFP can be interpreted as the coordinated stepping of multiple motor subunits in rapid succession, resulting in a “translocation burst.” Therefore, the nonlinear relationship between the pause-free translocation velocity and the mean GFP unfolding time may originate in the change in the probability of the motor making coordinated translocation steps with ATP concentration. Future experiments using optical tweezers with subnanometer resolution will make it possible to study the stepping behavior of the motor and may reveal a significant increase in the probability of coordinated steps among multiple motor subunits for ClpX relative to ClpXP as a function of nucleotide concentration.

Interestingly, the GFP unfolding intermediate observed in ClpX and in ClpXP single-molecule trajectories is essentially the same (59). This observation suggests that the unfolding pathway of GFP observed by the activity of ClpX or ClpXP is largely a reflection of the topology and energy landscape of the protein substrate. Although ClpX and ClpXP unfolded GFP via the same intermediate, their efficiency in unfolding the protein substrate was quite different. The unfolding efficiency of the enzyme is calculated from the ratio of rips corresponding to successful GFP unfolding events to the total number of rips (i.e., the summation of successful unfolding events and motor slips). We found that ClpXP was more efficient than ClpX at unfolding a protein substrate composed of two tandem GFP molecules (0.5 versus 0.2 efficiency, respectively) (59). In fact, ClpX displayed a much higher frequency of motor slips, wherein the motor apparently failed to unfold GFP, disengaged temporarily from the substrate, and moved backward along the polypeptide track (59). Several mechanisms can lead to better unfoldase activity of ClpX when it is bound to the peptidase ClpP. For instance, ClpP may stabilize the ClpX ring conformation (34), allowing a more stable grip on the protein substrate. Alternatively, the extended processing pore formed by the ClpXP complex can have additional interaction contacts with the unfolded protein substrate that may help prevent substrate release after an unsuccessful unfolding attempt.

EPILOGUE

To maintain a functional and efficient proteome, the cell must strike a balance ensuring the correct folding of polypeptides needed at any given state of its cycle and the timely removal of the protein complement it no longer needs in that state. This balance is attained by the coordinated activity of a large number of molecular machines. Starting at the time of birth of a polypeptide, this cellular machinery provides the binding interactions and energy expenditure necessary to guarantee its correct native folding, to avoid its trapping in nonfunctional and possibly cytotoxic aggregates, and to eliminate it when it is no longer functional or needed. Methods of single-molecule detection and manipulation are now systematically being used, as described in this review, to investigate the detailed operations of the individual components of this machinery. Future studies will likely involve the simultaneous characterization of several of these molecular machines to unravel their coordinated activities and the physical principles that underlie that coordination. The ability to combine single-molecule fluorescence detection and manipulation in the same experiment (23) will also enable researchers to monitor the displacement, force, and/or torque

generation of these machines, while simultaneously recording the dynamics of their internal degrees of freedom.

ACKNOWLEDGMENTS

C.J.B. acknowledges support from National Institutes of Health grant 5R01GM032543. C.M.K. acknowledges support from the QB3 California Institute for Quantitative Biosciences, Berkeley. D.H.G. acknowledges the National Science Foundation's graduate research fellowship. After this article was written, C.M.K. became affiliated with the Department of Biology at Johns Hopkins University, R.A.M. became affiliated with the Department of Chemistry at Georgetown University, and C.A.M.W. became affiliated with the Departamento de Bioquímica y Biología Molecular, Universidad de Chile, Santiago.

LITERATURE CITED

1. Abdelhakim AH, Oakes EC, Sauer RT, Baker TA. Unique contacts direct high-priority recognition of the tetrameric Mu transposase-DNA complex by the AAA+ unfoldase ClpX. Mol. Cell. 2008; 30:39–50. [PubMed: 18406325]
2. Adachi K, Oiwa K, Nishizaka T, Furuike S, Noji H, et al. Coupling of rotation and catalysis in F_1-ATPase revealed by single-molecule imaging and manipulation. Cell. 2007; 130:309–21. [PubMed: 17662945]
3. Bell GI. Models for the adhesion of cells to cells. Science. 1978; 200:618–27. [PubMed: 347575]
4. Aitken CE, Petrov A, Puglisi JD. Single ribosome dynamics and the mechanism of translation. Annu. Rev. Biophys. 2010; 39:491–513. [PubMed: 20192783]
5. Ashkin A. Acceleration and trapping of particles by radiation pressure. Phys. Rev. Lett. 1970; 24:156–59.
6. Ashkin A, Dziedzic JM, Bjorkholm JE, Chu S. Observation of a single-beam gradient force optical trap for dielectric particles. Opt. Lett. 1986; 11:288–90. [PubMed: 19730608]
7. Aubin-Tam ME, Olivares AO, Sauer RT, Baker TA, Lang MJ. Single-molecule protein unfolding and translocation by an ATP-fueled proteolytic machine. Cell. 2011; 145:257–67. [PubMed: 21496645]
8. Bechtluft P, van Leeuwen RG, Tyreman M, Tomkiewicz D, Nouwen N, et al. Direct observation of chaperone-induced changes in a protein folding pathway. Science. 2007; 318:1458–61. [PubMed: 18048690]
9. Bhushan S, Gartmann M, Halic M, Armache JP, Jarasch A, et al. α-Helical nascent polypeptide chains visualized within distinct regions of the ribosomal exit tunnel. Nat. Struct. Mol. Biol. 2010; 17:313–17. [PubMed: 20139981]
10. Bhushan S, Hoffmann T, Seidelt B, Frauenfeld J, Mielke T, et al. SecM-stalled ribosomes adopt an altered geometry at the peptidyl transferase center. PLoS Biol. 2011; 9:e1000581. [PubMed: 21267063]
11. Bhushan S, Meyer H, Starosta AL, Becker T, Mielke T, et al. Structural basis for translational stalling by human cytomegalovirus and fungal arginine attenuator peptide. Mol. Cell. 2010; 40:138–46. [PubMed: 20932481]
12. Blanchard SC, Cooperman BS, Wilson DN. Probing translation with small-molecule inhibitors. Chem. Biol. 2010; 17:633–45. [PubMed: 20609413]
13. Borgia A, Williams PM, Clarke J. Single-molecule studies of protein folding. Annu. Rev. Biochem. 2008; 77:101–25. [PubMed: 18412537]
14. Bustamante C. In singulo biochemistry: When less is more. Annu. Rev. Biochem. 2008; 77:45–50. [PubMed: 18518817]
15. Bustamante C, Chemla YR, Forde NR, Izhaky D. Mechanical processes in biochemistry. Annu. Rev. Biochem. 2004; 73:705–48. [PubMed: 15189157]
16. Bustamante C, Marko JF, Siggia ED, Smith S. Entropic elasticity of lambda-phage DNA. Science. 1994; 265:1599–600. [PubMed: 8079175]
17. Bustamante C, Macosko JC, Wuite GJ. Grabbing the cat by the tail: manipulating molecules one by one. Nat. Rev. Mol. Cell Biol. 2000; 1:130–36. [PubMed: 11253365]

18. Camberg JL, Hoskins JR, Wickner S. The interplay of ClpXP with the cell division machinery in *Escherichia coli*. J. Bacteriol. 2011; 193:1911–18. [PubMed: 21317324]
19. Cecconi C, Shank EA, Bustamante C, Marqusee S. Direct observation of the three-state folding of a single protein molecule. Science. 2005; 309:2057–60. [PubMed: 16179479]
20. Chakraborty K, Chatila M, Sinha J, Shi Q, Poschner BC, et al. Chaperonin-catalyzed rescue of kinetically trapped states in protein folding. Cell. 2010; 142:112–22. [PubMed: 20603018]
21. Chemla YR, Aathavan K, Michaelis J, Grimes S, Jardine PJ, et al. Mechanism of force generation of a viral DNA packaging motor. Cell. 2005; 122:683–92. [PubMed: 16143101]
22. Collin D, Ritort F, Jarzynski C, Smith SB, Tinoco I, Bustamante C. Verification of the Crooks fluctuation theorem and recovery of RNA folding free energies. Nature. 2005; 437:231–34. [PubMed: 16148928]
23. Comstock MJ, Ha T, Chemla YR. Ultrahigh-resolution optical trap with single-fluorophore sensitivity. Nat. Methods. 2011; 8:335–40. [PubMed: 21336286]
24. Crooks GE. Entropy production fluctuation theorem and the nonequilibrium work relation for free energy differences. Phys. Rev. E. 1999; 60:2721–26.
25. Deniz AA, Mukhopadhyay S, Lemke EA. Single-molecule biophysics: at the interface of biology, physics and chemistry. J. R. Soc. Interface. 2008; 5:15–45. [PubMed: 17519204]
26. Dong J, Castro CE, Boyce MC, Lang MJ, Lindquist S. Optical trapping with high forces reveals unexpected behaviors of prion fibrils. Nat. Struct. Mol. Biol. 2010; 17:1422–30. [PubMed: 21113168]
27. Dudko OK, Hummer G, Szabo A. Theory, analysis, and interpretation of single-molecule force spectroscopy experiments. Proc. Natl. Acad. Sci. USA. 2008; 105:15755–60. [PubMed: 18852468]
28. Elcock AH. Molecular simulations of cotranslational protein folding: fragment stabilities, folding cooperativity, and trapping in the ribosome. PLoS Comput. Biol. 2006; 2:e98. [PubMed: 16789821]
29. Ellis JP, Bakke CK, Kirchdoerfer RN, Jungbauer LM, Cavagnero S. Chain dynamics of nascent polypeptides emerging from the ribosome. ACS Chem. Biol. 2008; 3:555–66. [PubMed: 18717565]
30. Elms PJ, Chodera JD, Bustamante C, Marqusee S. The molten globule state is unusually deformable under mechanical force. Proc. Natl. Acad. Sci. USA. 2012; 109:3796–801. [PubMed: 22355138]
31. Fisher TE, Marszalek PE, Fernandez JM. Stretching single molecules into novel conformations using the atomic force microscope. Nat. Struct. Biol. 2000; 7:719–24. [PubMed: 10966637]
32. Frank J, Gonzalez RL Jr. Structure and dynamics of a processive Brownian motor: the translating ribosome. Annu. Rev. Biochem. 2010; 79:381–412. [PubMed: 20235828]
33. Glynn SE, Martin A, Nager AR, Baker TA, Sauer RT. Structures of asymmetric ClpX hexamers reveal nucleotide-dependent motions in a AAA+ protein-unfolding machine. Cell. 2009; 139:744–56. [PubMed: 19914167]
34. Glynn SE, Nager AR, Baker TA, Sauer RT. Dynamic and static components power unfolding in topologically closed rings of a AAA+ proteolytic machine. Nat. Struct. Mol. Biol. 2012; 19:616–22. [PubMed: 22562135]
35. Gorbatyuk B, Marczynski GT. Regulated degradation of chromosome replication proteins DnaA and CtrA in *Caulobacter crescentus*. Mol. Microbiol. 2005; 55:1233–45. [PubMed: 15686567]
36. Gottesman S, Roche E, Zhou Y, Sauer RT. The ClpXP and ClpAP proteases degrade proteins with carboxy-terminal peptide tails added by the SsrA-tagging system. Genes Dev. 1998; 12:1338–47. [PubMed: 9573050]
37. Hartl FU, Bracher A, Hayer-Hartl M. Molecular chaperones in protein folding and proteostasis. Nature. 2011; 475:324–32. [PubMed: 21776078]
38. Hinczewski M, Gebhardt JC, Rief M, Thirumalai D. From mechanical folding trajectories to intrinsic energy landscapes of biopolymers. Proc. Natl. Acad. Sci. USA. 2013; 110:4500–5. [PubMed: 23487746]

39. Hofmann H, Hillger F, Pfeil SH, Hoffmann A, Streich D, et al. Single-molecule spectroscopy of protein folding in a chaperonin cage. Proc. Natl. Acad. Sci. USA. 2010; 107:11793–98. [PubMed: 20547872]
40. Horwich AL, Weber-Ban EU, Finley D. Chaperone rings in protein folding and degradation. Proc. Natl. Acad. Sci. USA. 1999; 96:11033–40. [PubMed: 10500119]
41. Hoyt MA, Zich J, Takeuchi J, Zhang M, Govaerts C, Coffino P. Glycine-alanine repeats impair proper substrate unfolding by the proteasome. EMBO J. 2006; 25:1720–29. [PubMed: 16601692]
42. Hsu ST, Cabrita LD, Fucini P, Dobson CM, Christodoulou J. Structure, dynamics and folding of an immunoglobulin domain of the gelation factor (ABP-120) from *Dictyostelium discoideum*. J. Mol. Biol. 2009; 388:865–79. [PubMed: 19281823]
43. Hsu ST, Fucini P, Cabrita LD, Launay H, Dobson CM, Christodoulou J. Structure and dynamics of a ribosome-bound nascent chain by NMR spectroscopy. Proc. Natl. Acad. Sci. USA. 2007; 104:16516–21. [PubMed: 17940046]
44. Jarzynski C. Nonequilibrium equality for free energy differences. Phys. Rev. Lett. 1997; 78:2690–93.
45. Jiang Y, Douglas NR, Conley NR, Miller EJ, Frydman J, Moerner WE. Sensing cooperativity in ATP hydrolysis for single multisubunit enzymes in solution. Proc. Natl. Acad. Sci. USA. 2011; 108:16962–67. [PubMed: 21896715]
46. Kaiser CM, Chang HC, Agashe VR, Lakshmipathy SK, Etchells SA, et al. Real-time observation of trigger factor function on translating ribosomes. Nature. 2006; 444:455–60. [PubMed: 17051157]
47. Kaiser CM, Goldman DH, Chodera JD, Tinoco I Jr, Bustamante C. The ribosome modulates nascent protein folding. Science. 2011; 334:1723–27. [PubMed: 22194581]
48. Kenniston JA, Baker TA, Fernandez JM, Sauer RT. Linkage between ATP consumption and mechanical unfolding during the protein processing reactions of an AAA+ degradation machine. Cell. 2003; 114:511–20. [PubMed: 12941278]
49. Kenniston JA, Baker TA, Sauer RT. Partitioning between unfolding and release of native domains during ClpXP degradation determines substrate selectivity and partial processing. Proc. Natl. Acad. Sci. USA. 2005; 102:1390–95. [PubMed: 15671177]
50. Khushoo A, Yang Z, Johnson AE, Skach WR. Ligand-driven vectorial folding of ribosome-bound human CFTR NBD1. Mol. Cell. 2011; 41:682–92. [PubMed: 21419343]
51. Kim SY, Miller EJ, Frydman J, Moerner WE. Action of the chaperonin GroEL/ES on a non-native substrate observed with single-molecule FRET. J. Mol. Biol. 2010; 401:553–63. [PubMed: 20600107]
52. Kodera N, Yamamoto D, Ishikawa R, Ando T. Video imaging of walking myosin V by high-speed atomic force microscopy. Nature. 2010; 468:72–76. [PubMed: 20935627]
53. Kosolapov A, Deutsch C. Tertiary interactions within the ribosomal exit tunnel. Nat. Struct. Mol. Biol. 2009; 16:405–11. [PubMed: 19270700]
54. Kramer G, Boehringer D, Ban N, Bukau B. The ribosome as a platform for co-translational processing, folding and targeting of newly synthesized proteins. Nat. Struct. Mol. Biol. 2009; 16:589–97. [PubMed: 19491936]
55. Kramers HA. Brownian motion in a field of force and the diffusion model of chemical reactions. Physica. 1940; 7:284–304.
56. Li GW, Xie XS. Central dogma at the single-molecule level in living cells. Nature. 2011; 475:308–15. [PubMed: 21776076]
57. Liphardt J, Dumont S, Smith SB, Tinoco I Jr, Bustamante C. Equilibrium information from nonequilibrium measurements in an experimental test of Jarzynski's equality. Science. 2002; 296:1832–35. [PubMed: 12052949]
58. Lu J, Deutsch C. Folding zones inside the ribosomal exit tunnel. Nat. Struct. Mol. Biol. 2005; 12:1123–29. [PubMed: 16299515]
59. Maillard RA, Chistol G, Sen M, Righini M, Tan J, et al. ClpX(P) generates mechanical force to unfold and translocate its protein substrates. Cell. 2011; 145:459–69. [PubMed: 21529717]
60. Martin A, Baker TA, Sauer RT. Rebuilt AAA+ motors reveal operating principles for ATP-fuelled machines. Nature. 2005; 437:1115–20. [PubMed: 16237435]

61. Martin A, Baker TA, Sauer RT. Distinct static and dynamic interactions control ATPase-peptidase communication in a AAA+ protease. Mol. Cell. 2007; 27:41–52. [PubMed: 17612489]
62. Martin A, Baker TA, Sauer RT. Pore loops of the AAA+ ClpX machine grip substrates to drive translocation and unfolding. Nat. Struct. Mol. Biol. 2008; 15:1147–51. [PubMed: 18931677]
63. Martin A, Baker TA, Sauer RT. Protein unfolding by a AAA+ protease is dependent on ATP-hydrolysis rates and substrate energy landscapes. Nat. Struct. Mol. Biol. 2008; 15:139–45. [PubMed: 18223658]
64. Mashaghi A, Kramer G, Bechtluft P, Zachmann-Brand B, Driessen AJ, et al. Reshaping of the conformational search of a protein by the chaperone trigger factor. Nature. 2013; 500:98–101. [PubMed: 23831649]
65. Matouschek A, Bustamante C. Finding a protein's Achilles heel. Nat. Struct. Biol. 2003; 10:674–76. [PubMed: 12942137]
66. Mickler M, Dima RI, Dietz H, Hyeon C, Thirumalai D, Rief M. Revealing the bifurcation in the unfolding pathways of GFP by using single-molecule experiments and simulations. Proc. Natl. Acad. Sci. USA. 2007; 104:20268–73. [PubMed: 18079292]
67. Mickler M, Hessling M, Ratzke C, Buchner J, Hugel T. The large conformational changes of Hsp90 are only weakly coupled to ATP hydrolysis. Nat. Struct. Mol. Biol. 2009; 16:281–86. [PubMed: 19234469]
68. Moffitt JR, Chemla YR, Izhaky D, Bustamante C. Differential detection of dual traps improves the spatial resolution of optical tweezers. Proc. Natl. Acad. Sci. USA. 2006; 103:9006–11. [PubMed: 16751267]
69. Moffitt JR, Chemla YR, Smith SB, Bustamante C. Recent advances in optical tweezers. Annu. Rev. Biochem. 2008; 77:205–28. [PubMed: 18307407]
70. O'Brien EP, Christodoulou J, Vendruscolo M, Dobson CM. New scenarios of protein folding can occur on the ribosome. J. Am. Chem. Soc. 2011; 133:513–26. [PubMed: 21204555]
71. Oesterhelt F, Oesterhelt D, Pfeiffer M, Engel A, Gaub HE, Müller DJ. Unfolding pathways of individual bacteriorhodopsins. Science. 2000; 288:143–46. [PubMed: 10753119]
72. Pechmann S, Willmund F, Frydman J. The ribosome as a hub for protein quality control. Mol. Cell. 2013; 49:411–21. [PubMed: 23395271]
73. Pedersen S. *Escherichia coli* ribosomes translate in vivo with variable rate. EMBO J. 1984; 3:2895–98. [PubMed: 6396082]
74. Perez-Jimenez R, Garcia-Manyes S, Ainavarapu SR, Fernandez JM. Mechanical unfolding pathways of the enhanced yellow fluorescent protein revealed by single molecule force spectroscopy. J. Biol. Chem. 2006; 281:40010–14. [PubMed: 17082195]
75. Petrov A, Chen J, O'Leary S, Tsai A, Puglisi JD. Single-molecule analysis of translational dynamics. Cold Spring Harb. Perspect. Biol. 2012; 4:a011551. [PubMed: 22798542]
76. Qu X, Wen JD, Lancaster L, Noller HF, Bustamante C, Tinoco I Jr. The ribosome uses two active mechanisms to unwind messenger RNA during translation. Nature. 2011; 475:118–21. [PubMed: 21734708]
77. Ratzke C, Berkemeier F, Hugel T. Heat shock protein 90's mechanochemical cycle is dominated by thermal fluctuations. Proc. Natl. Acad. Sci. USA. 2012; 109:161–66. [PubMed: 22184223]
78. Ratzke C, Mickler M, Hellenkamp B, Buchner J, Hugel T. Dynamics of heat shock protein 90 C-terminal dimerization is an important part of its conformational cycle. Proc. Natl. Acad. Sci. USA. 2010; 107:16101–6. [PubMed: 20736353]
79. Rodrigo-Brenni MC, Hegde RS. Design principles of protein biosynthesis-coupled quality control. Dev. Cell. 2012; 23:896–907. [PubMed: 23153486]
80. Sauer RT, Baker TA. AAA+ proteases: ATP-fueled machines of protein destruction. Annu. Rev. Biochem. 2011; 80:587–612. [PubMed: 21469952]
81. Sauer RT, Bolon DN, Burton BM, Burton RE, Flynn JM, et al. Sculpting the proteome with AAA+ proteases and disassembly machines. Cell. 2004; 119:9–18. [PubMed: 15454077]
82. Siddiqui SM, Sauer RT, Baker TA. Role of the processing pore of the ClpX AAA+ ATPase in the recognition and engagement of specific protein substrates. Genes Dev. 2004; 18:369–74. [PubMed: 15004005]

83. Shank EA, Cecconi C, Dill JW, Marqusee S, Bustamante C. The folding cooperativity of a protein is controlled by its chain topology. Nature. 2010; 465:637–40. [PubMed: 20495548]
84. Sharma S, Hoskins JR, Wickner S. Binding and degradation of heterodimeric substrates by ClpAP and ClpXP. J. Biol. Chem. 2005; 280:5449–55. [PubMed: 15591068]
85. Smith SB, Cui Y, Bustamante C. Optical-trap force transducer that operates by direct measurement of light momentum. Methods Enzymol. 2003; 361:134–62. [PubMed: 12624910]
86. Stigler J, Ziegler F, Gieseke A, Gebhardt JC, Rief M. The complex folding network of single calmodulin molecules. Science. 2011; 334:512–16. [PubMed: 22034433]
87. Szyk A, Maurizi MR. Crystal structure at 1.9 Å of *E. coli* ClpP with a peptide covalently bound at the active site. J. Struct. Biol. 2006; 156:165–74. [PubMed: 16682229]
88. Takei Y, Iizuka R, Ueno T, Funatsu T. Single-molecule observation of protein folding in symmetric GroEL-$(GroES)_2$ complexes. J. Biol. Chem. 2012; 287:41118–25. [PubMed: 23048033]
89. Tinoco I Jr, Gonzalez RL Jr. Biological mechanisms, one molecule at a time. Genes Dev. 2011; 25:1205–31. [PubMed: 21685361]
90. Too PH, Erales J, Simen JD, Marjanovic A, Coffino P. Slippery substrates impair function of a bacterial protease ATPase by unbalancing translocation versus exit. J. Biol. Chem. 2013; 288:13243–57. [PubMed: 23530043]
91. Tu GF, Reid GE, Zhang JG, Moritz RL, Simpson RJ. C-terminal extension of truncated recombinant proteins in *Escherichia coli* with a 10Sa RNA decapeptide. J Biol. Chem. 1995; 270:9322–26. [PubMed: 7536743]
92. Weinkam P, Pletneva EV, Gray HB, Winkler JR, Wolynes PG. Electrostatic effects on funneled landscapes and structural diversity in denatured protein ensembles. Proc. Natl. Acad. Sci. USA. 2009; 106:1796–801. [PubMed: 19181849]
93. Wen JD, Lancaster L, Hodges C, Zeri AC, Yoshimura SH, et al. Following translation by single ribosomes one codon at a time. Nature. 2008; 452:598–603. [PubMed: 18327250]
94. Wilson DN, Beckmann R. The ribosomal tunnel as a functional environment for nascent polypeptide folding and translational stalling. Curr. Opin. Struct. Biol. 2011; 21:274–82. [PubMed: 21316217]
95. Woolhead CA, Johnson AE, Bernstein HD. Translation arrest requires two-way communication between a nascent polypeptide and the ribosome. Mol. Cell. 2006; 22:587–98. [PubMed: 16762832]
96. Xu AJ, Springer TA. Calcium stabilizes the von Willebrand factor A2 domain by promoting refolding. Proc. Natl. Acad. Sci. USA. 2012; 109:3742–47. [PubMed: 22357761]
97. Zaher HS, Green R. Fidelity at the molecular level: lessons from protein synthesis. Cell. 2009; 136:746–62. [PubMed: 19239893]
98. Zhang G, Ignatova Z. Folding at the birth of the nascent chain: coordinating translation with co-translational folding. Curr. Opin. Struct. Biol. 2011; 21:25–31. [PubMed: 21111607]
99. Zhou HX, Dill KA. Stabilization of proteins in confined spaces. Biochemistry. 2001; 40:11289–93. [PubMed: 11560476]

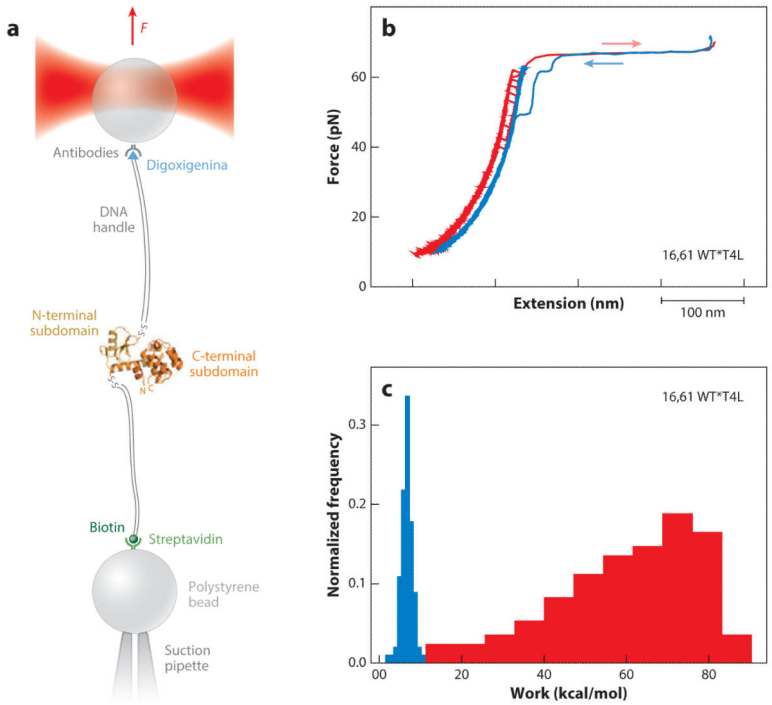

Figure 1.

Energetic coupling of subdomain folding in T4 lysozyme revealed by nonequilibrium single-molecule force spectroscopy. (*a*) Experimental setup. A T4 lysozyme protein is attached to polystyrene beads by means of DNA handles. The protein contains cysteines that permit covalent attachment to two 500–base pair double-stranded DNA molecular handles through disulfide linkages in only one domain of the protein. These DNA handles are derivatized on their 5′ ends with digoxigenin and biotin to bind the respective beads (antidigoxigenin-coated beads and streptavidin-coated beads, respectively). The streptavidin bead is attached to a micropipette by suction and has a diameter of 2.1 μm. This system is inside a laminar flow camera. Modified with permission from Reference 47. (*b*) Force-extension curves obtained by stretching (*red*) and relaxing (*blue*) a single domain of the T4 lysozyme; DNA handles were attached in the N domain of the protein. The data shown were collected at a 50-Hz sampling rate and a pulling speed of 60 nm/s. Reprinted with permission from Reference 83. (*c*) The normalized probability curves of unfolding and refolding work for 16,61 WT*T4L. The normalized probability curves of the work required for the unfolding (*red*) and refolding (*blue*) were obtained from the unfolding events in panel *b*. The Crooks fluctuation theorem (CFT) was used to calculate the free energy from the single-molecule experiments. The calculated free energy for 16,61 WT*T4L, obtained by the crossing point between the refolding and unfolding work (ΔG, CFT = 12.3 ± 0.6 kcal/mol), agrees well with the free energy measured in bulk solution unfolding experiments (ΔG, bulk = 14.1 ± 0.6 kcal/mol). Reprinted with permission from Reference 83. Abbreviations: pN, piconewton; T4L, T4 lysozyme; WT, wild type.

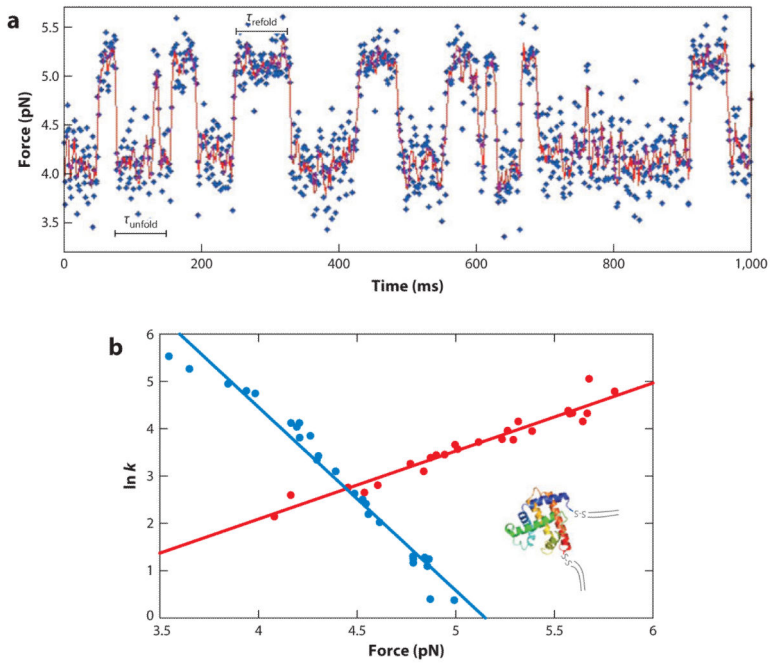

Figure 2.

Real-time observation of folding transitions in apomyoglobin. (*a*) Constant trap position experiments performed across the N and C termini of apomyoglobin H36Q. One-second trace of a constant trap position experiment at 1,000 Hz sampling frequency (*blue*) for the N- to C-terminal attachment points. The inferred trajectory of the molecule at 500 Hz is shown (*red*). The plot shows the lifetimes in each state at a particular force, and the protein "hops" between each state. (*b*) Linear fits of the natural logarithm (ln) of the rate constants as a function of force are shown for apomyoglobin. The distance to the transition state is determined from the slope of the lines using Bell's model [see the equation in the sidebar, Dependence of the Rate Constant on Force (Bell Equation)]. The $\Delta x^{\ddagger}_{unf} = 3.4 \pm 1.2$ nm, the $\Delta x^{\ddagger}_{fold} = 7.6 \pm 3.3$ nm, the Δx_{total} (sum of $\Delta x^{\ddagger}$) $= 11.0 \pm 3.5$ nm, and the Δx_{total} (measured in the optical tweezers instrument) $= 12 \pm 1$ nm. Adapted with permission from Reference 30. Abbreviation: pN, piconewton.

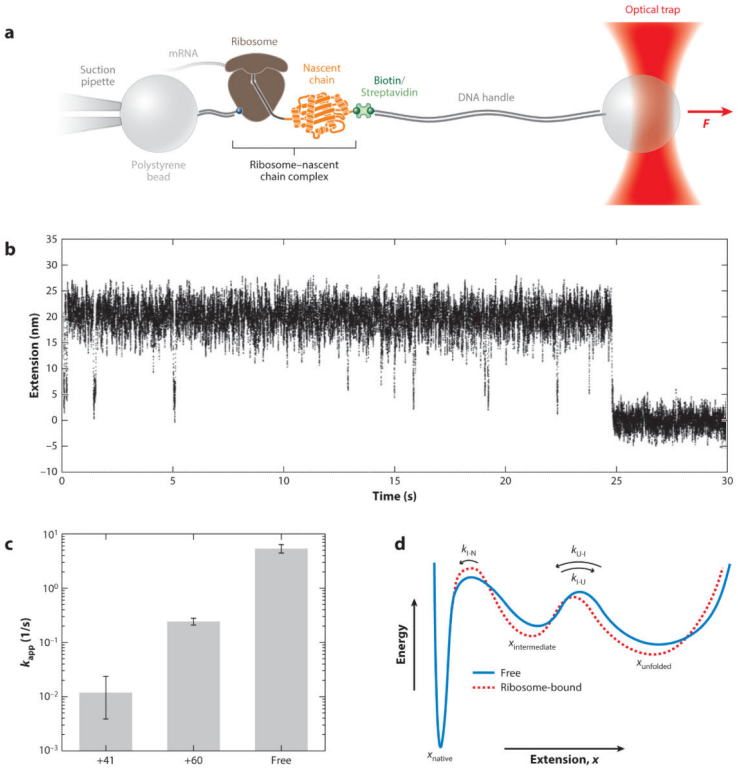

Figure 3.

Folding of ribosome-bound nascent polypeptides. (*a*) Experimental setup for optical tweezers measurements of ribosome-bound nascent proteins. A ribosome–nascent chain complex is tethered between two polystyrene microspheres via DNA handles. Attachment points are located on the large subunit of the ribosome and the N terminus of the nascent protein. The force applied to the assembly can be varied by moving the optical trap. (*b*) Representative force-clamp trace for the folding of a single ribosome-bound T4 lysozyme molecule. At the beginning, the force is lowered to 3.6 pN, and the extension is monitored over time. In this example, the protein folds after 25 s. Equilibrium “hopping” between the unfolded state and an intermediate state is also observed. (*c*) Apparent refolding rates for three constructs studied in the optical tweezers, which are referred to as +41, +60, and free, for the ribosome-bound T4 lysozyme with a 41–amino acid C-terminal linker, the ribosome-bound T4 lysozyme with a 60–amino acid C-terminal linker, and the T4 lysozyme in the absence of the ribosome, respectively. (*d*) Schematic energy landscape based on single-molecule experiments, illustrating how the ribosome affects folding. The height of the barrier between the intermediate and native state is affected by the ribosome. Figure adapted with permission from Reference 47. Abbreviation: pN, piconewton.

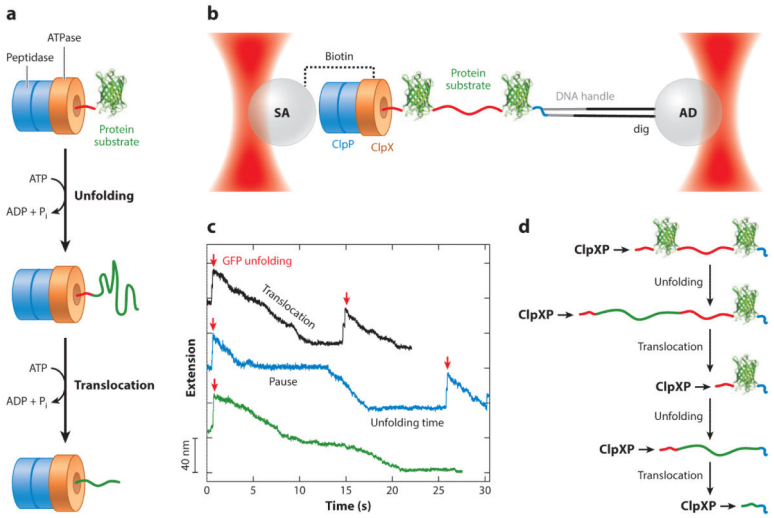

Figure 4.

Unfolding and translocation of protein substrates by ATP-dependent proteases monitored at the single-molecule level. (*a*) ClpXP binds, unfolds, and translocates ssrA-tagged protein substrates in an ATP-dependent manner. (*b*) Dual-trap optical tweezers assay to study protein unfolding and polypeptide translocation by individual ClpXP molecules. In this assay, ClpX is immobilized on the surface of a streptavidin (SA)-coated bead via a biotin-SA interaction. ClpP binds ClpX in *trans*. The DNA-tethered protein substrate has a digoxigenin (dig) molecule in one 5′ end of the DNA that binds to antidig (AD)-coated beads. The ssrA-tagged substrate consists of two green fluorescent protein (GFP) molecules separated by two permanently unfolded I27 titin domains (59). (*c*) Examples of molecular trajectories averaged down to 50 Hz showing protein unfolding and polypeptide translocation by ClpXP. Sudden gains in extension correspond to GFP unfolding events (*red arrowheads*). After unfolding, the gradual decrease in extension reflects the translocation of the unfolded polypeptide through the ClpX pore into ClpP. Occasionally, polypeptide translocation is interrupted by regions of near-zero velocity that were identified as pauses (*blue trajectory*). (*d*) Cartoon illustrating the sequence of events occurring in the molecular trajectories shown in panel *c*. Except for the green trajectory, ClpXP successfully unfolded both GFP molecules (59). Abbreviations: ATP, adenosine triphosphate; ssrA, small stable RNA A.

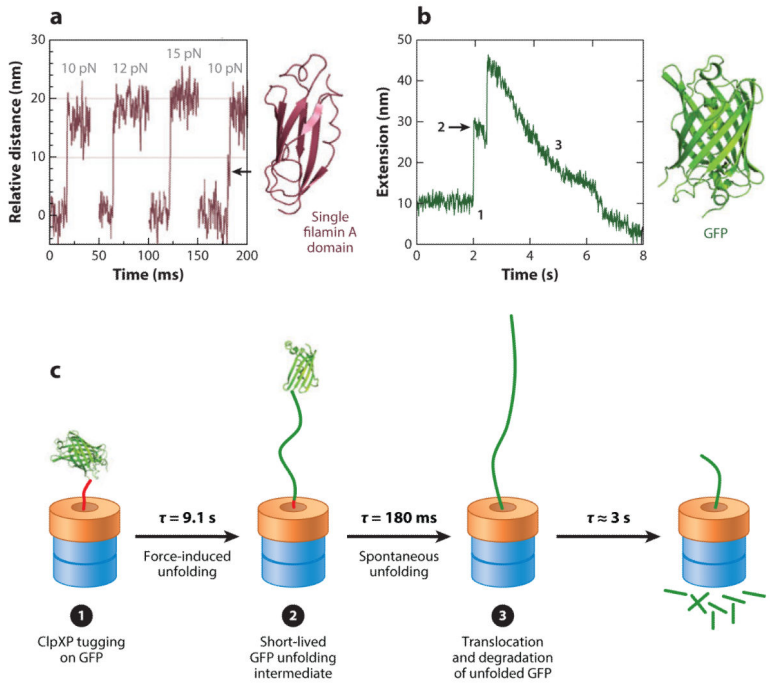

Figure 5.

Unfolding trajectories of protein substrates by ClpXP. (*a*) Rips corresponding to the cooperative unfolding of filamin A domains. The black arrow indicates the presence of a transient unfolding intermediate (7). (*b*) Green fluorescent protein (GFP) unfolding events were observed as a rip-transition-rip sequence, indicating the presence of an unfolding intermediate (*black arrow*). Numbers correspond to the sequence of events during GFP unfolding illustrated in panel *c*. (*c*) Model of GFP unfolding by ClpXP. ❶ After several unfolding attempts, ClpXP successfully extracts β-strands 11 through 7, generating an unfolding GFP intermediate. ❷ The remaining metastable intermediate unfolds spontaneously after ~180 ms. During the lifetime of the GFP intermediate, it is possible to monitor polypeptide translocation by ClpXP. ❸ After the complete unfolding of GFP, ClpXP continues translocating the unraveled polypeptide (59). Abbreviation: pN, piconewton; τ, lifetime.

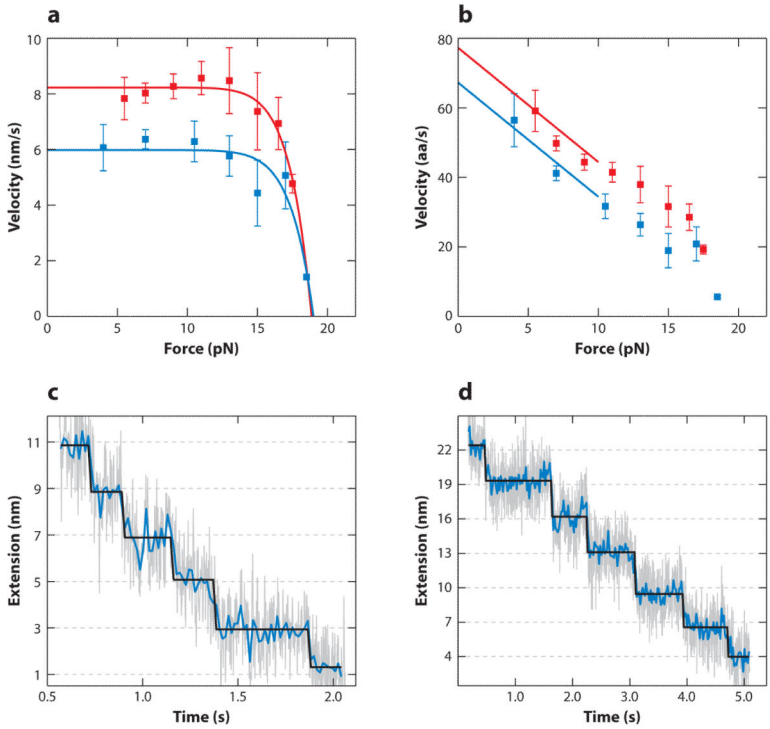

Figure 6.

Translocation velocity and stepping behavior of ClpXP. (*a*) Pause-free translocation velocity in nanometers per second as a function of force. Red and blue squares correspond to velocities for ClpX and ClpXP, respectively, here and in panel *b*. (*b*) Pause-free translocation velocity in amino acids (aa) per second as a function of force. (*c*,*d*) High-resolution data clearly displayed 2-nm or 3-nm steps during polypeptide translocation by ClpXP (*c* and *d*, respectively). Raw data (*gray*) were obtained at 2 kHz. The raw data were filtered down to 50 Hz (*blue*) and were fitted using a *t*-test step-detection algorithm (*solid black lines*). Figure adapted with permission from Reference 59.